Dalton Transactions

PAPER

View Article Online
View Journal | View Issue

Cite this: *Dalton Trans.*, 2018, **47**, 16279

Configurationally flexible zinc complexes as catalysts for *rac*-lactide polymerisation†

Pargol Daneshmand, Ina Michalsky, Pedro M. Aguiar and Frank Schaper *

Received 22nd June 2018,
Accepted 5th October 2018

DOI: 10.1039/c8dt02562b

rsc.li/dalton

$Zn(N(SiMe_3)_2)_2$ was reacted with pyridinemethanol and *R,R*–*N,N'*-di(methylbenzyl)-2,5-diiminopyrrole (**L1**H) to afford the dimeric complex $(\mathbf{L1})_2Zn_2(\mu\text{-}OR)_2$. The complex showed moderate activity in *rac*-lactide polymerization to heterotactic polymer (P_r = 0.75). 2,4-Di-*tert*-butyl-6-aminomethyl-phenol ligands with amino = *N,N,N',N'*-tetramethyldiethylenetriamine (**L2**H) or di-(2-picoly)amine (**L3**H) were reacted with $ZnEt_2$ to form (**L2**)ZnEt and with $Zn(N(SiMe_3)_2)_2$ to form the respective amide complexes. All complexes, including $(\mathbf{L1})_2Zn_2(\mu\text{-}OR)_2$ were characterised by X-ray diffraction studies. (**L2**)ZnEt was unreactive toward ethanol, but the amide complexes afforded (**L2**)ZnOEt and (**L3**)ZnOEt upon reaction with ethanol, which were used in *rac*-lactide polymerization without isolation. All complexes racemise readily at room temperature and show apparent C_s-symmetry in their NMR spectra. The ethoxide complexes were highly active in lactide polymerization, with (**L3**)ZnOEt reaching full conversion in 15 min at 0.5 mM catalyst concentration at room temperature. In both cases, introduction of a second donor arm on the central nitrogen introduced a slight bias for isotactic monomer enchainment (P_m = 0.55–0.60), which for (**L3**)ZnOEt was dependent on catalyst concentration.

Introduction

Using polylactic acid (PLA) as a green replacement for petroleum based resources has gained a lot of interest recently.[1–10] PLA is prepared through ring opening polymerisation (ROP) of lactide which itself is obtained through fermentation of corn starch.[11–13] Fuelled by its industrial application, controlled lactide polymerisation has become a catalytic challenge.[14–42] To date, there is no catalytic system which can polymerize lactide with high stereocontrol (P_m > 95%) (Scheme 1), excellent polymer molecular weight control and good activities under industrially relevant conditions (140–180 °C, in the presence of water and lactic acid).

The situation is rendered more interesting (and made thoroughly more complicated) by the number of possible mechanistic pathways for lactide polymerisation: in addition to ring-opening polymerisation by anionic or neutral organic initiators, lactide can be polymerized by Lewis-acid activation of the monomer together with a suitable co-initiator (alcohol) or by coordination–insertion polymerisation into a metal alkoxide catalyst. The same mechanistic multitude is observed for isotactic stereocontrol – which seems currently to be the biggest challenge: not only are the traditional stereocontrol mechanisms, chain-end and catalytic-site control, both observed in lactide polymerisation (sometimes opposing each other), but other mechanisms, such as selective chain transfer, can be operative.[43–45] In this context, there is growing evidence that in some instances a higher flexibility of the catalytic site can be beneficial, which is untypical for "traditional" stereocontrol mechanisms. Based on initial observations by Ma, Okuda and Carpentier,[46,47] and follow-up work of Davidson and Jones,[48–51] a *catalytic-site mediated (or ligand mediated) chain-end control* mechanism was proposed. While the chiral information is still derived from the polymer chain end, the latter does not interact directly with the incoming monomer. Rather, the catalytic site adapts its configuration to match the chirality of the chiral chain end, and in turn determines stereochemistry by interaction with the monomer. A flexible and preferably chiral catalytic site is a prerequisite for this mechanism.

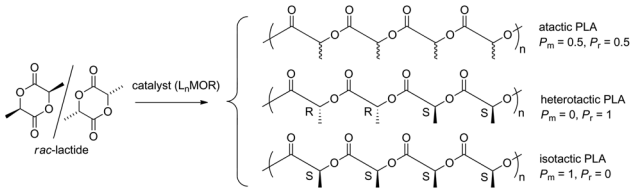

Scheme 1

Centre in Green Chemistry and Catalysis, Department of chemistry, Université deMontréal, C. P. 6128 Succ. Centre-Ville, Montréal, QC H3 T 3J7, Canada. E-mail: Frank.Schaper@umontreal.ca

†Electronic supplementary information (ESI) available: Additional details on polymerisation reactions, X-ray structures and NMR spectra. CCDC 1850465–1850469. For ESI and crystallographic data in CIF or other electronic format see DOI: 10.1039/c8dt02562b

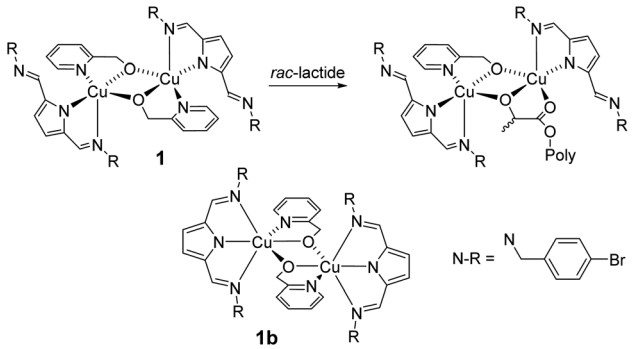

Scheme 2

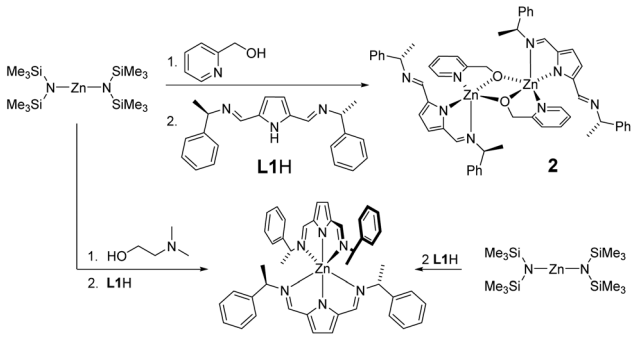

Scheme 3

We have recently observed this mechanism to be active in copper diiminopyrrolide complexes to provide moderately isotactic PLA.[52–55] The active species of catalyst **1** is found to be a dinuclear species, in which the penta-coordinated copper centres are chiral, but can readily racemise due to the presence of the pendant imino ligand (Scheme 2). Stereocontrol seemed to be largely invariant of the nature of the *N*-substituent, but a pyridylmethoxide ligand was essential. The only pyridylmethoxide complex which did not provide isotactic PLA, **1b** (Scheme 2), showed an octahedrally coordinated copper in its crystal structure and thus an achiral catalytic site, unable to participate in the proposed mechanism.

Due to their abundance, low price, non-toxicity and general lack of colour, zinc-based complexes have been expansively investigated in homogenous lactide polymerisation from the very beginning.[56,57] Zinc-based complexes typically show good to excellent activities and good polymer molecular weight control. But despite numerous studies,[14,15,17,20,24,26] including our own,[58] stereocontrol toward isotactic PLA was difficult to achieve. Only in recent years, zinc-catalysts with preference for isotactic monomer insertion emerged.[59–73] In the following, we explore if the stereocontrol mechanism observed in copper diiminopyrrolide complexes can be transferred to zinc-based catalysts, either using the identical ligand framework as for copper or by designing a catalyst capable of catalytic site racemisation.

Results and discussion

Diiminopyrrolide complexes

Synthesis and structure. Synthesis of **L1**H (Scheme 3) has been reported previously.[50] The dimeric complex $(\mathbf{L1})_2Zn_2(\mu\text{-}OCH_2C_5H_4N)_2$, **2**, was obtained similar to the analogous copper(II) complexes by reaction of zinc bis–bis(trimethylsilyl) amide with one equivalent of pyridinemethanol, followed by addition of the ligand **L1**H (Scheme 3).[50] If dimethylaminoethanol was used instead of pyridinemethanol, the corresponding homoleptic complex $(\mathbf{L1})_2Zn$ was obtained. For the sake of comparison and characterisation, $(\mathbf{L1})_2Zn$ was also prepared from reaction of $Zn(N(SiMe_3)_2)_2$ with two equivalents of **L1**H (see Fig. S1† for its crystal structure).

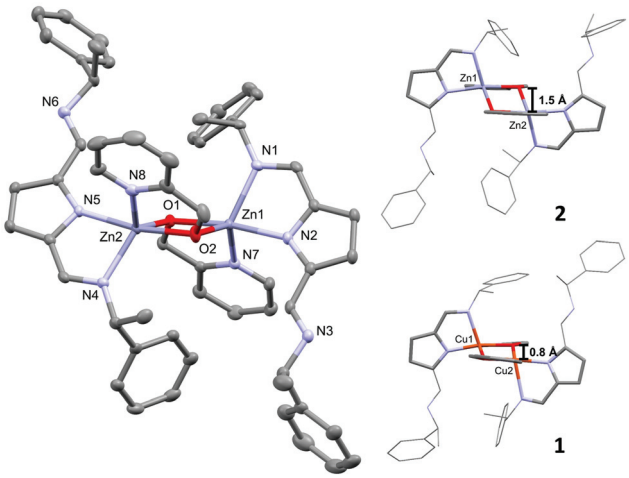

Fig. 1 X-ray structure of **2**. Thermal ellipsoids are drawn at the 50% probability level. Hydrogen atoms omitted for clarity.

Complex **2** crystallised as a dimeric, pentacoordinated complex, with distorted bipyramidal geometry around zinc (τ = 0.7,[74] Fig. 1). While τ-values can be misleading, this agrees with the observed metal–ligand bond lengths. In the distorted square-pyramidal coordination of **1**, the ligand in the apical position showed a notably (0.2–0.3 Å) elongated bond (Table 1). In distorted bipyramidal **2**, all zinc–ligand bond distances fall all in the range of 2.0–2.1 Å, irrespective of position,

Table 1 Selected geometric data for pyridylmethoxide complexes **1** and **2**[a]

	1[b]	**2**
$M–N_{Pyrrole}$	1.945(2), 1.964(2)	2.084(2), 2.0896(19)
$M–N_{imine}$	2.294(3), 2.242(3)	2.1205(19), 2.1095(18)
$M–O_{short}$	1.915(2), 1.944(2)	1.9908(16), 1.9850(15)
$M–O_{long}$	1.960(2), 1.960(2)	2.0744(16), 2.0666(17)
$M–N_{Pyridine}$	2.025(3), 1.995(3)	2.1084(19), 2.112(2)
M–M	3.025(5)	3.1091(4)
τ	0.6, 0.4	0.7, 0.7

[a] The second values cited refers to the second metal center of the dimer. [b] Taken from ref. 52 for comparison.

and are comparable to what has been reported in literature.[75] Overall though, the structure of **2** resembles very strongly that of **1** (Table 1, Fig. 1). Due to the differences in preferred coordination geometry, **1** showed a better defined equatorial complex plane with an offset of appr. 0.8 Å between the $CuON_2$-planes of each metal centre.[49] The structure of **2** is slightly more distorted, with a larger offset (appr. 1.5 Å) between the $ZnON_2$-planes.‡

The ^{1}H-NMR spectrum agrees with the unsymmetrical coordination of the ligand observed in the crystal structure: two sets of chemical shifts are obtained for the methylbenzylimino-substituent and the protons of pyrrole and of the methylene group are diastereotopic (Fig. S15†).

***rac*-Lactide polymerisation.** Despite the strong structural resemblance between **1** and **2**, polymerisation results with **2** were unsatisfactory and differed strongly from those of **1**. At room temperature and in C_6D_6 solution, complex **1** showed slow initiation (t_0 = 11 min), followed by pseudo-first order kinetics to produce moderately isotactic PLA after appr. 5 h (k_{obs} = 0.6 ± 0.1 h^{-1} at 2 mM catalyst concentration). Complex **2** likewise followed a pseudo-first order regime, but did not show an induction period. Instead, an apparent negative *x*-axis intercept of the regression curve at t_0 = −45 min indicated a higher rate of monomer consumption in the very first minutes of the polymerization. After this initial fast reaction, the reaction required 48 h to reach completion (k_{obs} = 0.15(1) h^{-1} at 2 mM catalyst concentration, Fig. 2) and produced moderately *heterotactic* PLA (P_r = 0.75). Polymer weight control is very poor, with appr. 5 chains produced per catalyst dimer and a high polydispersity of 2.8. The MALDI spectrum of the polymer shows the presence of cyclic oligomers from intramolecular transesterification (Fig. S6†). We thus cannot determine if only one (as in **1**) or if both pyridylmethoxide ligands initiate chain growth.

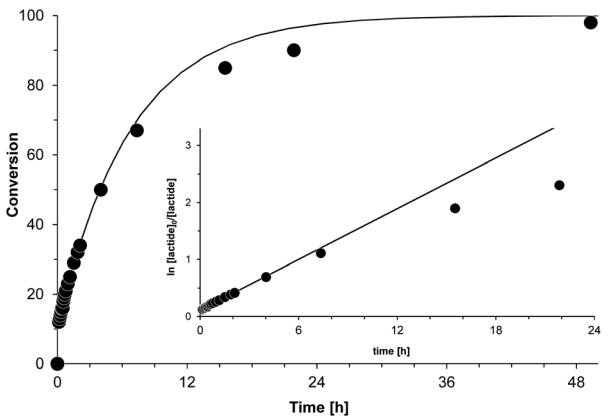

Fig. 2 Conversion-time profile for *rac*-lactide polymerisation with **2**. The inset shows the semi-logarithmic plot. Solid lines represent theoretical curves based on linear regression of the linear region in the semi-logarithmic plot. Conditions: [**2**] = 2.0 mM, [lactide] = 0.20 M, C_6D_6, RT. Final conversion : 98% after 48 h, M_n(GPC) = 3.0 kg mol^{-1}, M_w/M_n = 2.8.

‡As an alternative description of the two differing geometries, we can define the equatorial complex plane as containing M, O and N_{pyrrol}. The pyridylmethoxide ligands have an angle of 46°–48° with this plane (*cf.* 26°–30° in **1**) and the imino-pyrrolide ligands of 53°–62° (*cf.* 69°–82° in **1**).

Triaminophenolate complexes

Given the poor performance of the diiminopyrrolide complex, we decided to explore if stereocontrol *via site-mediated chain-end control* can be achieved with a ligand better suited for zinc. In 2003, Williams, Hillmyer, Tolman and coworkers reported a tetra-coordinated, monomeric Zn(II) catalyst carrying a diaminophenolate ligand (**3**, Scheme 4).[76] **3** is among the most active zinc-based catalysts reported, reaching full conversion in only 5 min at room temperature with good polymer molecular weight control and low polydispersities. The PLA produced was atactic, however. The high activity was attributed to reversible coordination of the pendant dimethylamino group. Polyamino-phenolate based ligands have been in the following well studied in zinc-catalysed lactide polymerisation.[59,62,69–72,77–83] Several strategies have been employed to add isotactic stereocontrol to this catalyst system. Mehrkhodavandi introduced chirality into the side arm and replaced the ethylene bridge with a chiral cyclohexylene bridge (**4**, Scheme 4).[84] The more rigid bridge, however, drastically reduced activity (full conversion in about 40 h), while the resulting PLA remained atactic. Removing the methyl group on the central nitrogen, increased activity, but did not improve on stereocontrol.[81] Ma added an aniline donor arm to the central amine donor (**5**, Scheme 4).[69] Stereocontrol correlated with the coordination environment of the zinc centre, with aniline-coordinated complexes providing heterotactic and amine-coordinated complexes providing isotactic PLA. The same group also successfully explored replacing the dimethylamino substituent with chiral or non-chiral cyclic amines to provide isotactic PLA.[71,72] The results are mechanistically complex and involve catalytic-site control and chain-end control active at the same time. More recently, Kol added a pyridylmethyl donor on the terminal amino group to form a tetradentate ligand with either achiral or chiral spacers (**6**, Scheme 4). The

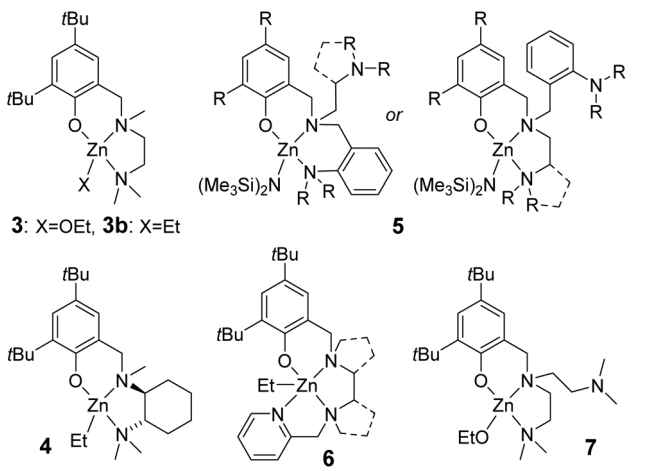

Scheme 4

complexes were highly active in polymerisation and provided isotactic PLA.[70,73] All these approaches relied on stabilizing a specific environment of the catalytic site. We decided to investigate whether deliberate introduction of flexibility into **3**, *i.e.* providing a stereochemically *unstable* catalytic site, would allow isotactic stereocontrol *via* a *catalytic-site mediated chain-end control* mechanism. Complex **7**, containing identical aminoethyl substituents should preserve the high activity of **3**, while exchange of the coordinating arms would invert chirality at the zinc and the central nitrogen atom simultaneously, and would allow facile racemisation of the complex (Scheme 4).

Syntheses and structures. **L2**H was prepared by reductive amination of 2-formyl-4,6-*tert*-butylphenol in the presence of $NaBH_3(CN)$ and acetic acid in methanol, adapting protocols for similar ligands.[78] It has been previously prepared by reaction of sodium dimethyl amide with the respective chloride substituted precursor.[85] Reaction of zinc diethyl with one equiv. of **L2**H produced a yellow oil from which colourless crystals of (**L2**)ZnEt, **8**, could be obtained (Scheme 5). The X-ray structure of **8** shows a chiral, tetrahedral Zn(II) complex in which only one of the dimethylamino arms is coordinated to the metal (Fig. 3). As hypothesised, the additional donor arm does not influence complex geometry, and **8** is essentially isostructural to **3b** (Scheme 4, Table 2).[76]

The ^{1}H NMR spectrum of **8** displays a higher apparent symmetry than its crystal structure (Fig. S20†). The two dimethylamino-capped side arms exchange readily on the NMR time scale and only one singlet is observed for all NMe_2 groups.§ More importantly, the $ArCH_2N$ group appears as a singlet with an intensity of 2 at 3.39 ppm. The side arm exchange is thus correlated with an inversion at the zinc centre *and* the central nitrogen, *i.e.* an racemisation of the complex, which renders these two protons homotopic (Scheme 5). It should be noted that complex **3b** shows two distinct singlets for the NMe_2 group and a pair of doublets for $ArCH_2N$ in its NMR spectrum.[76] Mehrkhodavandi showed that addition of pyridine led to coalescence of the NMe_2 signals, but the $ArCH_2N$ protons remained diastereotopic.[84] Racemisation thus does not occur in **3b** – even in the presence of Lewis bases – since it would require dissociation of both amine ligands at the same time. As envisioned, the presence of an additional donor arm in **8** facilitates epimerisation at the metal centre, a prerequisite for the targeted stereocontrol mechanism.

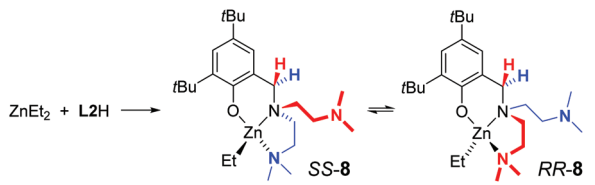

Scheme 5

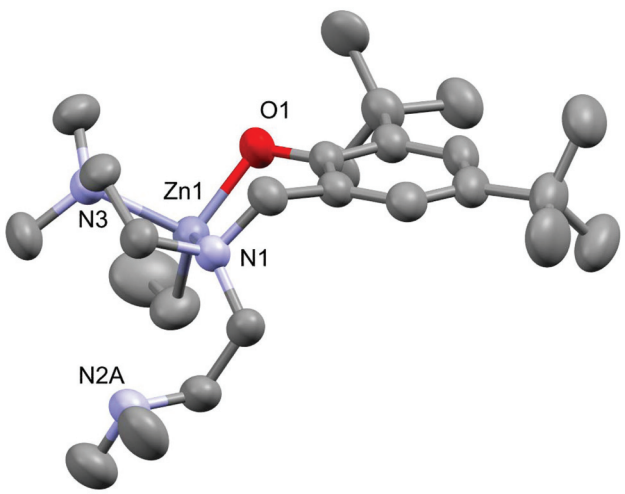

Fig. 3 X-ray structure of **8**. Thermal ellipsoids are drawn at the 50% probability level. Hydrogen atoms and minor fractions of disorder in *tert*-butyl and dimethylaminoethylene substituents omitted for clarity.

Williams *et al.* reported facile transformation of ethyl complex **3b** into the desired alkoxide complex **3** with ethanol. Unfortunately, the ethyl group in **8** was unreactive toward alcoholysis and, even after heating, NMR spectra confirmed the presence of unreacted **8** and ethanol. Similar problems were encountered in the reaction of **4** with ethanol,[84] and we and others have noticed previously that alcoholysis of the second zinc ethyl bond can be challenging.[58,86] In fact, the major product of $ZnEt_2$ in isopropanol is EtZnOiPr.[87] Zinc amide complexes are a commonly employed alternative pathway to prepare heteroleptic zinc alkoxides.[56] Complex **9** was thus prepared by addition of 1 equiv. $Zn(N(SiMe_3)_2)_2$ to a toluene solution of **L2**H, and formed colourless crystals after recrystallisation from hexane (Scheme 6).

The X-ray structure of **9** shows the same distorted tetrahedral coordination with one uncoordinated amine ligand as in **8** (Fig. 4, Table 2). The ^{1}H NMR spectrum of **9** likewise showed a single singlet for the aryl methylene group and one singlet for all dimethylamino groups, in agreement with fast exchange of coordinated and uncoordinated dimethylamine ligand, coupled with an epimerisation of the metal centre (Fig. S22†). Only one signal is observed for the trimethylsilyl substituents. $Zn–N_{amide}$ rotation is thus fast on the NMR time scale, but this process is not connected with complex racemisation.

The desired catalyst **7**, containing an alkoxide as a suitable initiator for *rac*-lactide polymerisation, was prepared by the addition of 1 equiv. of ethanol to a C_6D_6 solution of **9** (Scheme 6). The reaction was followed by ^{1}H NMR to ensure clean conversion to the alkoxide complex. The reaction was complete before the first NMR spectrum was taken (<10 min, Fig. S8†). As for the amide complexes, only one singlet is observed for the dimethylamine groups and the arylmethylene group, respectively, indicating fast epimerisation at the metal

§The same spectrum would be expected for a C_s-symmetric penta-coordinated complex, but it is highly unlikely to observe a higher coordination in solution than in the solid state.

Table 2 Geometrical details for the X-ray structures of **8–11**

	8	3b[a]	9	11
Zn–O	1.959(2)	1.956(3)	1.949(2), 1.941(2)	1.972(1)
Zn–$N_{terminal}$ [b]	2.159(3)	2.128(3)	2.154(3), 2.158(3)	2.210(1), 2.223(6)
Zn–NR_3	2.171(3)	2.147(4)	2.118(2), 2.124(2)	2.306(1)
Zn–C/N_{amide}	1.977(4)	1.998(4)	1.927(2), 1.933(3)	1.974(1)
O–Zn–C/N_{amide}	126.5(1)	128.8(1)	115.6(1), 116.0(1)	120.45(1)
O–Zn–$N_{terminal}$ [b]	101.6(1)	99.8(1)	103.4(1), 103.3(1)	95.49(4), 99.7(2)

[a] Taken from ref. 76. [b] $N_{terminal}$: NMe_2 (**3b**, **8**, **9**), pyridine (**11**).

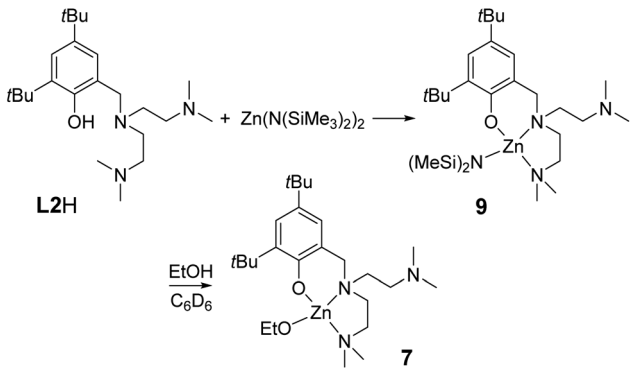

Scheme 6

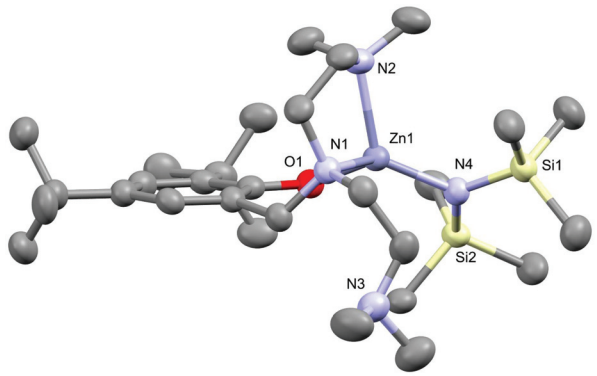

Fig. 4 X-ray structure of **9**. Thermal ellipsoids are drawn at the 50% probability level. Hydrogen atoms and the second, independent molecule in the asymmetric unit omitted for clarity.

centre. After ^{1}H NMR confirmed full conversion, C_6D_6 solutions of **7** were used as stock solutions in polymerisations experiments.

***rac*-Lactide polymerisation.** Complex **7** readily polymerized lactide in C_6D_6 solution at room temperature and reached full conversion after appr. 30 min at 2 mM catalyst concentration (Table 3). The catalyst follows clean first-order kinetics, without notable induction period or complex decomposition (Fig. 5). The pseudo-first-order rate constant at 2 mM catalyst concentration is k_{obs} = 4.1(1) h^{-1} (Fig. 5). Complex **7** was thus able to retain the high activity of complex **3**. The slightly lower rate when compared to **3** (k_{obs}(**3**) = 15 h^{-1} at [**3**] = 2 mM)[76] can be partly attributed to the difference in solvent (C_6D_6 here, CH_2Cl_2 for **3**) and partly to the presence of two diamino groups in **7**, which make dissociation of a diamino ligand, speculated to be required for lactide coordination,[76] statistically less likely. Unfortunately, **7** shows relatively poor polymer molecular weight control with polydispersities of 2.8 and a lower than expected polymer molecular weight. The MALDI spectrum of the polymer confirmed the presence of intramolecular transesterification reactions (Fig. S7 and S8†). The latter could be improved under immortal polymerisation conditions: in presence of 4 equiv. EtOH, **7** produced PLA with the expected molecular weight and lower polydispersities. Activity in immortal polymerisation was only half as high (Table 3, Fig. S2 and S3†), which is surprising since the complex should not be sensitive towards alcohol. PLA produced with **7** showed a very slight isotactic bias of P_m = 0.55. Using our standardised integration protocol (see Experimental part), P_m values are typically consistent to ±1% through-out a kinetic experiment and to ±3% in repeated experiments. The small amount of isotacticity observed is thus outside of typically experimental error, but might nevertheless be influenced by transesterification.[58] P_m values did, however, not show any variation with conversion or time and are thus not due to transesterification reactions (Fig. 6).

Dipyridylaminophenolate complexes

Syntheses and structures. To compare the influence of catalytic site racemisation on stereocontrol, *rac*-lactide polymerisation was investigated with **10**, in which the dimethyl amino donors were replaced with pyridyl (Scheme 7). Complexes similar to **10** have been briefly investigated by Thomas and Carpentier and produced atactic PLA.[78] **10** was prepared analogous to **7**: reaction of $Zn(N(SiMe_3)_2)_2$ and **L3H** provided the amide complex **11**. Further reaction with ethanol in C_6D_6 afforded **10**, which was directly used in polymerisation (Scheme 7). In contrast to **8** and **9**, in the crystal structure of **11** both pyridine ligands were coordinated to the metal centre (Fig. 7). A τ-value of 0.1 would indicate square-pyramidal geometry, but closer inspection of the structure and the respective metal–ligand bond lengths propose distorted bipyramidal geometry as a better description (Table 2). The structure of **11** does not show mirror-symmetry, despite the coordination of both pyridine ligands, since the geometry of the aryl methylene group forces a bending of the aryl group out of the ZnN_2-

Table 3 *rac*-Lactide polymerisation with **7** and **10**[a]

	Catalyst	[cat.]	[Lactide]	Zn : lactide	Final conversion (time)	k_{obs}	M_n [b]	M_n [c] (calc.)	M_w/M_n	Chains/Zn[d]	P_m [e]
1	**7**	2.0 mM	200 mM	1 : 100	99% (420 min)	4.1(1) h^{-1}	6.0 kDa	14.3 kDa	2.8	2.4	0.55
2	7 + 4 EtOH	2.0 mM	200 mM	1 : 100	99% (100 min)	2.5(1) h^{-1}	2.7 kDa	2.9 kDa	1.2	5	0.55
3	**7**	0.5 mM	50 mM	1 : 100	67% (100 min)	0.73(1) h^{-1}	9.1 kDa	9.6 kDa	1.1	1	0.55
4	**10**	2.0 mM	200 mM	1 : 100	97% (2 min)		2.4 kDa	14.0 kDa	1.9	5.8	0.49
5					99% (2 min)	120(3) h^{-1}	9.6 kDa	14.3 kDa	1.1	1.5	0.50
6	**10**	0.5 mM	50 mM	1 : 100	93% (20 min)	6.9(2) h^{-1}	33.8 kDa	13.4 kDa	1.9	0.4	0.55
7	**10**	0.5 mM	200 mM	1 : 400	96% (13 min)	12.2(6) h^{-1}	32.8 kDa	55.3 kDa	1.7	1.7	0.55
8	**10**	0.5 mM	500 mM	1 : 1000	60% (24 h)	0.9(1) h^{-1}	36.5 kDa	86.4 kDa	1.2	2.7	0.55
9	**10**	0.3 mM	150 mM	1 : 500	40% (16 h)	0.25(4) h^{-1}	23.2 kDa	27.4 kDa	1.2	1.2	0.60

[a] Conditions: C_6D_6, RT. [b] M_n and M_w determined by size exclusion chromatography *vs.* polystyrene standards, with a Mark–Houwink correction factor of 0.58. [c] Calculated from [lactide]/([cat] + [EtOH])·conversion·$M_{lactide}$ + M_{ROH}. [d] Number of chains per zinc centre, calculated from the ratio of expected and obtained polymer molecular weight. [e] P_m determined from decoupled ^{1}H NMR by $P_m = 1 - 2{\cdot}I_1/(I_1 + I_2)$, with I_1 = 5.20–5.25 ppm (*rmr*, *mmr*/*rmm*), I_2 = 5.13–5.20 ppm (*mmr*/*rmm*, *mmm*, *mrm*).

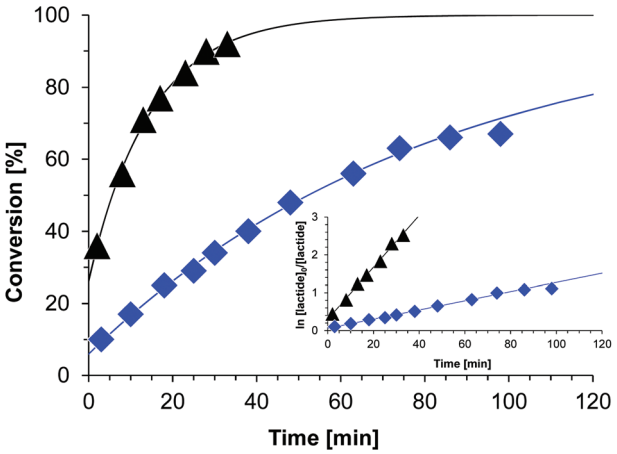

Fig. 5 Conversion-time profiles for *rac*-lactide polymerisation with **7**. Conditions: C_6D_6, RT, **7** : lactide = 1 : 100. The inset shows the semi-logarithmic plot. Solid lines correspond to theoretical conversions based on rate constants obtained from linear regression: black triangles: [**7**] = 2.0 mM, k_{obs} = 4.1(1) h^{-1}, t_0 = −5 min, final conversion after >7 h: 99%; blue diamonds: [**7**] = 0.5 mM, k_{obs} = 0.73(1) h^{-1}, t_0 = −5 min, final conversion after >7 h: 67%. The negative axis intercept might indicate partial catalyst decomposition in the first 5 min of the reaction, inhomogeneous starting conditions or – although unlikely – experimental error.

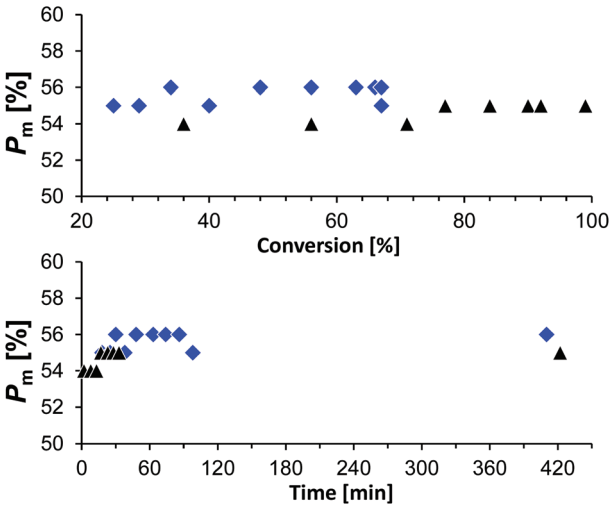

Fig. 6 Variation of polymer microstructure (P_m) in dependence of conversion or time in *rac*-lactide polymerisations with **7**. Black triangles: [**7**] = 2.0 mM, blue diamonds: [**7**] = 0.5 mM. With [**7**] = 0.5 mM, conversion plateaued at 67%.

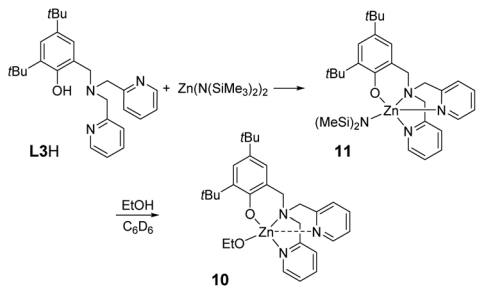

Scheme 7

plane toward one of the pyridine ligands. The latter shows a bending of the Zn–$N_{Pyridine}$ bond out of the mean plane of the pyridine to allow closer contact with the aryl group, indicating favourable π-interactions between the two aromatic systems (angle between planes = 34°, shortest atom-plane contact = 3.0 Å).

The ^{1}H NMR spectrum of **11** likewise shows indications of stronger interaction of pyridine with the zinc centre. While **11** still displays apparent C_s-symmetry in its ^{1}H spectrum, peaks are broadened, indicative of a lower rate of exchange: the $PyCH_2$ groups appear as one broadened and one sharp doublet and the $ArCH_2$ group is broadened to a large peak between 3.8–4.9 ppm (Fig. S26†). Only one set of pyridine signals are observed, significantly broadened and coupling is barely visible. **11** thus either exists in solution as a tetrahedral complex and undergoes slow racemisation (Scheme 8, **A**), or it interchanges between a tetrahedral and a five-coordinated species by dissociation/recoordination of a pyridine ligand (**B**), or the complex remains five-coordinated, with a slow "flipping" of the phenolate ring (**C**). All these dynamic processes

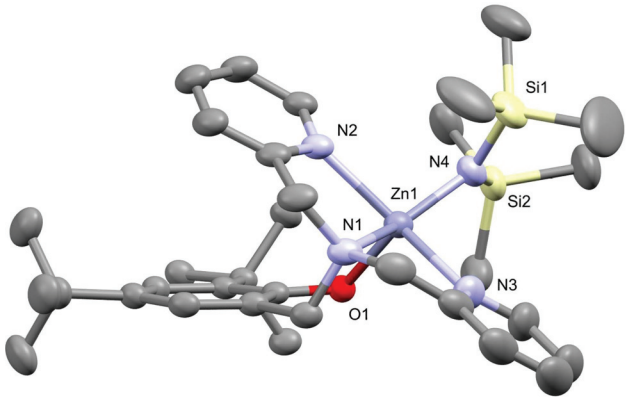

Fig. 7 X-ray structure of **11**. Thermal ellipsoids are drawn at the 50% probability level. Hydrogen atoms, and the second, independent molecule in the asymmetric unit omitted for clarity.

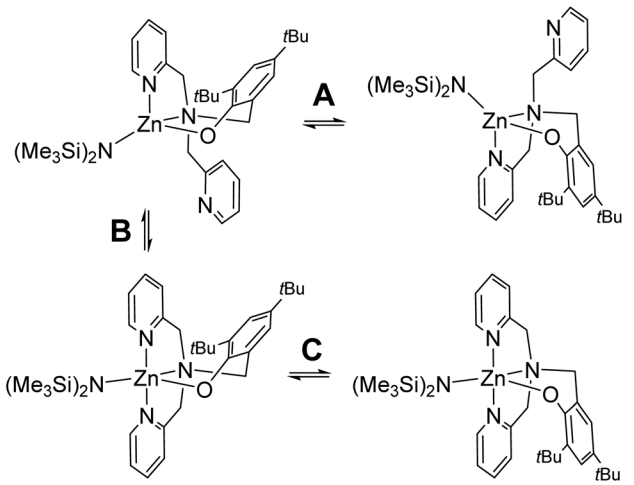

Scheme 8

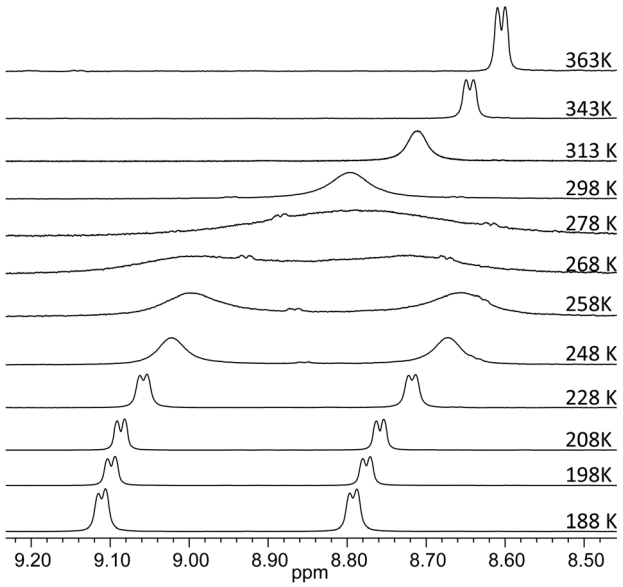

Fig. 8 Variable temperature NMR spectra of **11** showing the coalescence of the *ortho* hydrogen atoms of the two pyridyl units (see ESI† for further spectra).

generate apparent C_s-symmetry and equalize the two pyridyl moieties. Derivatives of **11**, previously reported by Thomas and Carpentier,[78] likewise showed apparent C_s-symmetry in their NMR spectra. At higher temperatures, peaks of **11** sharpen to yield the apparently C_s-symmetric spectrum. Below 250 K, the spectrum shows one species with independent signal sets for each of the pyridylmethylene arms (Fig. 8 and S32–S35†). The trimethylsilyl signal likewise splits into two peaks at lower temperatures. However, while activation barriers estimated from the coalescence temperatures of the aromatic and methylene protons fall in the range of $\Delta G^{\ddagger}$ = 53–57 kJ mol^{-1}, an activation barrier of $\Delta G^{\ddagger} \approx 46$ kJ mol^{-1} is obtained for the trimethylsilyl signals. The latter is thus an unrelated kinetic process, probably involving rotation around the Zn–N bond. Upon irradiation of the pyridyl *ortho* hydrogen atoms at 9.1 and 8.8 ppm, respectively, an NOE enhancement of the trimethylsilyl signal was observed for both hydrogen atoms. However, only irradiation of the hydrogen atom at 8.8 ppm showed an NOE enhancement of the *tert*-butyl group at 1.8 ppm. These observations agree best with the species at low temperature being the five-coordinated Zn complex, observed in the crystal structure. The kinetic process observed in the NMR spectra is thus most likely the "flipping" of the phenolate ring (Scheme 8, **C**).

The ^{1}H NMR spectra of the respective ethoxide complex **10** shows essentially the same features as **11**: only one set of peaks for the pyridyl ligands in agreement with apparent C_s symmetry, but with overall broadened peaks (Fig. S11†). Regardless of the exact nature of the dynamic process, racemisation – if it happens at all in **10** and **11** – is more difficult with pyridyl donors than with dimethylamine ligands.

***rac*-Lactide polymerisation.** Complex **10** was highly active in lactide polymerisation (Table 3). Polymerisation was completed in 2 min at ambient temperature at 2 mM catalyst concentration and in appr. 15 min at 0.5 mM, placing **10** among the most active zinc-based catalysts (*cf.* estimated k_{obs} at 2 mM [Zn]: **3**,[76] 15 h^{-1}; **5**,[69] 10 h^{-1}; **6**,[73] 50 h^{-1}; **7**, 4 h^{-1}; **10**, 120 h^{-1}). No induction period was observed, but regression curves of kinetics at 0.5 mM all showed a negative *x*-axis intercept, indicative of catalyst deactivation at the beginning of the reaction (Fig. S4 and S5†). The same was observed for **7**, but only to an extent still explicable by experimental error. While decomposition did not visually affect polymerisations at catalyst : lactide ratios of 1 : 100 or 1 : 400, polymerisations at a ratio of 1 : 1000 or at catalyst concentrations of 0.3 mM showed curved semi-logarithmic plots and did not reach completion, indicative of catalyst decomposition before the end of the reaction (Fig. S4 and S5†). At 0.1 mM catalyst concentration, we did not observe more than 10% conversion. Polymerisation with **7** at reduced catalyst concentrations (0.5 mM) also failed to reach completion (Fig. 5, Table 3). Polydispersities of PLA

produced with **10** varied between 1.1 to 1.9, but in most cases the polymer molecular weight was smaller than expected. MALDI spectra of the polymer showed the presence of cyclic oligomers, indicative again of intramolecular transesterification (Fig. S10–S14†).

While PLA obtained with **7** showed slight isotacticity (P_m = 0.55, Table 3), PLA produced with **10** was atactic (P_m = 0.49–0.50, Table 3). This would be in line with a higher tendency of pyridine to coordinate to zinc and the proposed catalytic-site mediated chain-end control: if the active species is a penta-coordinated zinc complex, the catalytic site is achiral and cannot transfer the chirality of the chain-end to zinc. In diiminopyrrolide copper complexes of type **1**, the only complex ever observed to coordinate both iminogroups to form an achiral catalytic site (**1b**, Scheme 2) was also the only complex of type **1** producing atactic PLA.[54,55] Alternatively, the catalytic site might be slow to racemise and to adapt to the chain-end, also resulting in loss of the ability to transfer chain-end chirality to the monomer. In the latter case, stereocontrol can be influenced by reaction conditions, since insertion is dependent on monomer concentration, while – in first approximation – catalyst racemisation is not. At lower monomer concentrations, the ratio of racemisation *vs.* insertion rate will thus be higher. If lactide concentration was reduced from 200 to 50 mM, while keeping the lactide : catalyst ratio constant, stereocontrol indeed increased to P_m = 0.55 (Table 3). Closer investigation revealed, however, that this effect was not due to reduced lactide concentration, but rather due to reduced catalyst concentrations: increasing the lactide concentration to 200 or even to 500 mM, while keeping the catalyst concentration at 0.5 mM, did not affect stereocontrol, which remained constant at P_m = 0.55 (Table 3). On the other hand, lowering the catalyst concentration to 0.3 mM increased stereocontrol further to P_m = 0.60. For **7**, lowering of the catalyst concentration did not affect stereocontrol (Table 3). There are several mechanistic explications for a negative impact of catalyst concentration on stereocontrol, such as chain-exchange between centres in a catalytic-site control mechanism or the formation of dinuclear species with different reactivities. Given the overall low isoselectivity of **7** and **10**, in particular when compared to **5** and **6**, and the mediocre polymer molecular weight control, we did not investigate this issue further.

Conclusions

The application of the ligand system which provided isotactic copper-based polymerisation catalysts to zinc, afforded a complex of surprisingly similar structure, but strongly different polymerisation reactivity. Metals with coordination geometries closer to copper might show more similar reactivity, but our attempts to prepare the respective iron, cobalt or manganese complexes have not been successful so far.

For aminophenolate-based complexes, the counterintuitive approach to provide additional flexibility to the catalytic site and enable fast racemisation was successful in introducing a slight isotactic bias in one of the most active zinc-based catalysts. While the low isotacticity and poor polymer molecular weight control do not encourage further optimisation of this ligand system in particular, these results underline that lactide polymerisation often defies the axiom that successful control requires a rigid environment of the catalytic site and that catalytic sites with flexible conformation or even flexible configuration might offer an alternative approach to achieve stereocontrol.

Experimental

General considerations

All reactions were carried out using Schlenk or glove box techniques under nitrogen atmosphere. $Zn(N(SiMe_3)_2)_2$,[88] 2,4-di-*tert*-butylsalicyladehyde,[89] *N*,*N*,*N*,*N*-tetramethyldiethylenetriamine,[90] and **L1**H,[53] were prepared according to literature. Solvents were dried by passage through activated aluminum oxide (MBraun SPS), de-oxygenated by repeated extraction with nitrogen, and stored over molecular sieves. C_6D_6 was dried over molecular sieves. *rac*-Lactide (98%) was purchased from Sigma–Aldrich, purified by 3× recrystallisation from dry ethyl acetate and kept at −30 °C. All other chemicals were purchased from common commercial suppliers and used without further purification. ^{1}H and ^{13}C NMR spectra were acquired on Bruker Advance 300 and 400 spectrometers. Chemical shifts were referenced to the residual signals of the deuterated solvents ($CDCl_3$: ^{1}H: δ 7.26 ppm, ^{13}C: δ 77.16; C_6D_6: 1H: δ 7.16 ppm, ^{13}C: δ 128.06 ppm). Elemental analyses were performed by the Laboratoire d'analyse élémentaire (Université de Montréal). All UV-Vis measurements were performed in degassed and anhydrous toluene at RT in a sealed quartz cell on a Cary 500i UV-Vis-NIR Spectrophotometer.

2,4-Di-*tert*-butyl-6-((*N*,*N*,*N*′,*N*′-tetramethyldiethylenetriamine)) phenol, L2H.[85] A procedure from literature was adapted as follows:[78] To a brown mixture of 3,5-di-*tert*-butyl-2-hydroxybenzaldehyde (0.50 g, 2.1 mmol), $NaBH_3(CN)$ (0.16 g, 2.5 mmol) and a few drops of acetic acid in methanol (10 ml), was added a solution of *N*,*N*,*N*,*N*-tetramethyldiethylenetriamine (0.67 g, 4.2 mmol) in methanol (10 ml) dropwise. The reaction was stirred for 48 h. The methanol was evaporated and the resulting brown residue was purified by silica gel chromatography (2% MeOH, 1% NEt_3 in $CHCl_3$) yielding a light yellow oil (0.62 g, 78%).

^{1}H NMR ($CDCl_3$, 300 MHz): δ 7.18 (d, J = 3 Hz, 1H, Ar), 6.82 (d, J = 3 Hz, 1H, Ar), 3.74 (s, 2H, $ArCH_2N$), 2.68–2.63 (m, 2H, CH_2), 2.47–2.43 (m, 2H, CH_2), 2.19 (s, 12H, $N(CH_3)_2$), 1.40 (s, 9H, CH_3), 1.27 (s, 9H, CH_3); ^{13}C{^{1}H} NMR ($CDCl_3$, 75 MHz): δ 154.3 (Ar), 140.4 (Ar), 129.8 (Ar), 123.9 (Ar), 122.9 (Ar), 121.9 (Ar), 59.0 (CH_2), 57.1 (CH_2), 51.9 (CH_2), 45.8 ($N(CH_3)_2$), 35.0 ($C(CH_3)_3$), 34.2 ($C(CH_3)_3$), 31.8 (CH_3), 29.7 (CH_3). ESI-HRMS (m/z): $[M + H]^+$ ($C_{23}H_{44}N_3O$) calcd 378.3478; found 378.3485.

2,4-Di-*tert*-butyl-6-((di-(2-picolyl)amine)phenol, L3H. A procedure from literature was slightly modified as follows:[78] Analogous to **L2**H, from 3,5-di-*tert*-butyl-2-hydroxybenzalde-

hyde (0.50 g, 2.1 mmol), $NaBH_3(CN)$ (0.16 g, 2.5 mmol), a few drops of acetic acid, di-(2-picoly)amine (0.84 g, 4.2 mmol) in methanol (20 ml) stirred for 4 hours to yield a brown residue which was purified by silica gel chromatography (2% MeOH, 1% NEt_3 in $CHCl_3$) (0.34 g, 39%).

^{1}H NMR ($CDCl_3$, 300 MHz): δ 10.62 (s, 1H, OH), 8.56 (ddd, J = 6, 2, 1 Hz, 2H, Py), 7.63 (td, J = 8, 2 Hz, 2H, Py), 7.37 (d, J = 8 Hz, 2H, Py), 7.20 (d, J = 3 Hz, 1H, Ar), 7.15 (ddd, J = 8, 6, 1 Hz, 2H, Py), 6.87 (d, J = 3 Hz, 1H, Ar), 3.87 (s, 4H, $PyCH_2N$), 3.80 (s, 2H, $ArCH_2N$), 1.45 (s, 9H, CH_3), 1.26 (s, 9H, CH_3); ^{13}C{^{1}H} NMR ($CDCl_3$, 75 MHz): δ 158.3 (Py), 154.0 (Ar), 149.2 (Py), 140.5 (Ar), 136.7 (Py), 135.7 (Ar), 124.7 (Ar), 123.7 (Py), 123.3 (Ar), 122.4 (Py), 121.8 (Ar), 59.7 (CH_2), 58.4 (CH_2), 35.1 ($C(CH_3)_3$), 34.2 ($C(CH_3)_3$), 31.8 (CH_3), 29.8 (CH_3). ESI-HRMS (m/z): $[M + H]^+$ ($C_{27}H_{36}N_3O$) calcd 418.2852; found 418.2857.

(L1)$_2$Zn$_2$(μ-O,κ$_N$-OCH$_2$C$_6$H$_2$N)$_2$, 2. $Zn(N(SiMe_3)_2)_2$ (115 mg, 0.304 mmol) was suspended in toluene (3 ml). 2-Pyridinemethanol (28.3 μl, 0.304 mmol) was added to the red suspension, which was left to stir for 45 min. A freshly prepared light orange solution of **L1**H (100 mg, 0.304 mmol) in toluene (2 ml) was added dropwise, resulting in a light yellow solution. The reaction was stirred 24 hours at RT, filtered to remove trace impurities, concentrated to 1/3 of the volume resulting in colourless crystals. The crystals were separated by decantation and washed with ether (3 × 10 ml) (23 mg, 16%).

^{1}H NMR (C_6D_6, 400 MHz): δ 8.18 (s, 1H, (N═C)H), 7.80 (s, 1H, (N═C)H), 7.35 (s, 1H), 7.29 (bs, 2H, Ph), 7.04–6.95 (m, 3H), 6.95–6.83 (m, 5H), 6.76 (s, 1H), 6.65 (t, J = 8 Hz, 1H), 6.15 (d, J = 8 Hz, 1H, pyrrole), 4.64 (d, J = 18 Hz, 1H, $PyCH_2$), 4.56 (d, J = 18 Hz, 1H, $PyCH_2$), 4.24 (q, J = 7 Hz, 1H, CH), 4.10 (q, J = 7 Hz, 1H, CH), 1.50 (d, J = 7 Hz, 3H, CH_3), 1.20 (d, J = 7 Hz, 3H, CH_3); ^{13}C{^{1}H} NMR (C_6D_6, 101 MHz): δ 165.2 ((N═C)H), 157.0 (Ar), 154.8 ((N═C)H), 146.7 (Ar), 145.9 (Ar), 144.6 (Ar), 141.6 (Ar), 140.2 (Ar), 137.4 (Ar), 129.3 (Ar), 128.5 (Ar), 127.4 (Ar), 127.0 (Ar), 126.9 (Ar), 126.7 (Ar), 122.0 (Ar), 120.9 (Ar), 116.3 (Ar), 115.7 (Ar), 68.4 (CH_2), 67.7 (CH), 64.2 (CH), 24.7 (CH_3), 24.6 (CH_3). UV-vis (toluene, 2.2 × 10^{-6} M) [λ_{max}, nm (ε, mol^{-1} cm^2)]: 378 (23 500), 387 (23 800). Anal. calcd for $C_{56}H_{56}Zn_2N_8O_2$: C, 67.00; H, 5.62; N, 11.16; found: C, 66.34; H, 5.62; N, 10.65.

(L1)$_2$Zn. $Zn(HMDS)_2$ (115 mg, 0.304 mmol) was suspended in toluene (3 ml). A freshly prepared light orange solution of **L1**H (200 mg, 0.608 mmol) in toluene (2 ml) was added dropwise, resulting in a light yellow solution. The reaction was stirred 24 hours at RT, filtered to remove trace impurities, concentrated to 1/3 of the volume resulting in colourless crystals. The crystals were separated by decantation and washed with ether (3 × 10 ml) and recrystallised two times from a mixture of toluene : hexane (1 : 3) (53 mg, 24%).

^{1}H NMR (C_6D_6, 400 MHz): δ 7.80 (s, 2H, (N═C)H), 7.04–6.98 (m, 6H, Ph), 6.93–6.86 (m, 4H, Ph), 6.76 (s, 2H, 3,4-Pyrrole), 4.10 (q, J = 7 Hz, 2H, CH), 1.20 (d, J = 7 Hz, 6H, CH_3). UV-vis (toluene, 2.2 × 10^{-6} M) [λ_{max}, nm (ε, mol^{-1} cm^2)]: 376 (20 600), 389 (22 000), 433 (sh). Despite X-ray quality crystals and repeated re-crystallizations, a satisfactory elemental analysis could not be obtained. The NMR likewise indicates the presence of impurities.

(L2)ZnOEt, 7. To a solution of **9** (10 mg, 16 μmol) in C_6D_6 (0.6 ml) in a J-Young tube was added a freshly prepared solution of EtOH in C_6D_6 (0.20 M) in two portions of appr. 40 μL. The reaction was followed by NMR and the amount of the second batch of ethanol was adjusted with regard to remaining **9**. After NMR confirmed complete replacement of the amide by ethoxide, the solution used directly in polymerization.

^{1}H NMR (C_6D_6, 400 MHz,): δ 7.64 (d, J = 3 Hz, 1H, Ar), 6.94 (d, J = 3 Hz, 1H, Ar), 3.25 (s, 2H, $ArCH_2$), 2.11 (s, 12 H, NMe_2), 2.01–2.08 (m, 2H, CH_2), 1.96 (ddd, J = 13, 9, 4 Hz, 2H, CH_2), 1.90 (s, 9H, CMe_3), 1.73 (m, 2H, CH_2), 1.45–1.60 (m, 7H, CH_3 + 2 CH_2), 1.50 (s, 9H, CMe_3); ^{13}C{^{1}H} NMR (C_6D_6, 101 MHz): δ 165.4 (Ar), 138.5 (Ar), 134.3 (Ar), 125.5 (Ar), 124.2 (Ar), 121.9 (Ar), 59.9 (CH_2Ar), 55.9 (CH_2), 51.2 (CH_2), 46.3 (NMe_2), 45.5 ($ZnOCH_2$), 35.9 (CMe_3), 34.2 (CMe_3), 32.4 (CMe_3), 32.1 ($ZnOCH_2Me$), 30.4 (CMe_3).

(L2)ZnEt, 8. $ZnEt_2$ (33 mg, 0.26 mmol) was added to a freshly prepared light yellow solution of **L2**H (100 mg, 0.26 mmol) in toluene (5 ml), resulting in an orange solution. The reaction was stirred 24 hours at RT, and filtered to remove trace impurities. The solvent was removed under vacuum and the resulting orange oil was crystallised from hexane (10 ml) at −30 °C. The colourless crystals were separated by decantation and washed with hexane (3 × 10 ml) (45 mg, 38%).

^{1}H NMR (C_6D_6, 400 MHz): δ 7.63 (d, J = 3 Hz, 1H, Ar), 6.97 (d, J = 3 Hz, 1H, Ar), 4.34 (bs, 2H, NCH_2), 3.39 (s, 2H, $ArCH_2N$), 2.50–2.40 (m, 2H, NCH_2), 2.37–2.21 (m, 4H, NCH_2), 1.89 (s, 21H, $C(CH_3)_3$ + $N(CH_3)_2$), 1.68 (t, J = 8 Hz, 3H, $ZnCH_2CH_3$), 1.49 (s, 9H, $C(CH_3)_3$), 0.45 (q, J = 8 Hz, 2H, $ZnCH_2$); ^{13}C{^{1}H} NMR (C_6D_6, 101 MHz): 155.2 (Ar), 133.6 (Ar), 131.5 (Ar), 124.4 (Ar), 123.0 (Ar), 58.3 (CH_2), 57.2 (CH_2), 51.4 (CH_2), 45.5 ($N(CH_3)_2$), 35.5 (CMe_3), 34.4 (CMe_3), 32.1 (CMe_3), 30.11 (CMe_3), 19.2 (CH_2Me), 1.4 ($ZnCH_2$). UV-vis (toluene, 1.2 × 10^{-4} M) [λ_{max}, nm (ε, mol^{-1} cm^2)]: 302 (2700). Anal. calcd for $C_{25}H_{47}ZnN_3O$: C, 63.75; H, 10.06; N, 8.92; found: C, 63.63; H, 10.25; N, 8.84.

(L2)ZnN(SiMe$_3$)$_2$, 9. Analogous to **8**, from $Zn(N(SiMe_3)_2)_2$ (102 mg, 0.265 mmol), **L2**H (100 mg, 0.265 mmol) in toluene (5 ml). Filtration, removal of the solvent under vacuum, crystallisation in hexane (10 ml) at −30 °C, decantation and washing with hexane (3 × 10 ml) afforded 52 mg (32%) of colourless X-ray quality crystals.

^{1}H NMR (C_6D_6, 400 MHz): δ 7.62 (d, J = 3 Hz, 1H, Ar), 6.87 (d, J = 3 Hz, 1H, Ar), 3.60 (s, 2H, $ArCH_2N$), 2.45 (dt, J = 11, 6 Hz, 2H, CH_2), 2.27 (td, J = 11, 6 Hz, 4H, CH_2), 2.08–1.98 (br m, 2H, CH_2), 1.93 (s, 12H, $N(CH_3)_2$), 1.78 (s, 9H, CH_3), 1.47 (s, 9H, CH_3), 0.49 (s, 18H, $Si(CH_3)_3$); ^{13}C{^{1}H} NMR (C_6D_6, 101 MHz): δ 164.4 (Ar), 138.1 (Ar), 134.9 (Ar), 126.3 (Ar), 124.9 (Ar), 120.7 (Ar), 62.1 (CH_2Ar), 56.6 (CH_2), 53.5 (CH_2), 46.7 ($N(CH_3)_2$), 35.9 (CMe_3), 34.2(CMe_3), 32.4 (CMe_3), 30.6 (CMe_3), 7.2 ($SiMe_3$). UV-vis (toluene, 7.6 × 10^{-5} M) [λ_{max}, nm (ε, mol^{-1} cm^2)]: 302 (4000). Anal. calcd for $C_{29}H_{60}N_4OSi_2Zn{\cdot}1/3C_6H_{14}$ C, 59.00; H, 10.33; N, 8.88; found: C, 59.25; H, 10.74; N, 9.16.

(L3)ZnOEt, 10. Analogous to **7**, from a freshly prepared solution of EtOH in C_6D_6 (0.20 M) and **11** (10 mg, 16 μmol). After NMR confirmed complete replacement of the amide by ethoxide, the solution used directly in polymerization.

^{1}H NMR (C_6D_6, 400 MHz,): δ 9.42 (br s, 2H, Py), 7.60 (s, 1H, Ar), 6.97 (s, 1H, Ar), 6.77 (t, J = 8 Hz, 2H, Py), 6.56 (t, J = 8 Hz, 2H, Py), 6.15 (bs, 2H, Py), 3.41 (bs, 2H, CH_2), 3.2–3.7 (br, 2H, CH_2), 2.75 (bs, 1H), 2.24 (bs, 1H), 1.91 (s, 9H, CMe_3), 1.6–1.8 (bm, 2H), 1.51 (s, 9H, CMe_3), 1.4 (bm, 3H); $^{13}C\{^1H\}$ NMR (C_6D_6, 101 MHz): δ 165.7 (Ar), 155.6 (Ar), 151.1 (Ar), 139.4 (Ar), 138.5 (Ar), 133.7 (Ar), 125.8 (Ar), 124.3 (Ar), 123.3 (Ar), 122.5 (Ar), 121.6 (Ar), 59.4 (CH_2Ar), 58.6 ($ZnOCH_2$), 57.2 (CH_2Py), 36.0 ($C(CH_3)_3$), 34.2 ($C(CH_3)_3$), 32.5 (CH_3), 32.0 ($ZnOCH_2CH_3$), 30.3 (CH_3).

(L3)ZnN(SiMe$_3$)$_2$, 11. Analogous to **8**, from $Zn(N(SiMe_3)_2)_2$ (92 mg, 0.24 mmol), **L3**H (100 mg, 0.24 mmol) in toluene (5 ml). Filtration, removal of the solvent under vacuum, crystallisation in hexane at −30 °C, decantation and washing with hexane (3 × 10 ml) afforded 54 mg (31%) of colourless X-ray quality crystals, containing 1 equiv. co-crystallised hexane.

^{1}H NMR (C_6D_6, 400 MHz, 298 K): δ 8.78 (bs, 2H, Py), 7.12 (d, J = 3 Hz, 1H, Ar), 6.79 (bs, 2H, Py), 6.62 (d, J = 3 Hz, 1H, Py), 6.50 (bs, 2H, Py), 6.27 (bs, 2H, Py), 3.72 (d, J = 14 Hz, 2H, $PyCH_2N$), 3.45 (d, J = 14 Hz, 2H, $PyCH_2N$), 3.29 (bs, 2H, $ArCH_2N$), 1.68 (s, 9H, CH_3), 1.32 (s, 9H CH_3), 0.50 (s, 18H, Si$(CH_3)_3$); ^{1}H NMR (C_7D_8, 500 MHz, 208 K): δ 9.09 (d, J = 5 Hz, 1H, *ortho* Py), 8.76 (d, J = 5 Hz, 1H, *ortho* Py′), 7.12 (d, J = 3 Hz, 1H, Ar), 6.83 (app. t, J = 7 Hz, 1H, *para* Py), 6.63 (d, J = 2 Hz, 1H, Ar), 6.55 (dt, J = 8, 1 Hz, 1H, *para* Py′), 6.50 (dd, J = 7, 6 Hz, 1 H, *meta* Py), 6.32 (m, 2H, *meta* Py, Py′), 5.98 (d, J = 8 Hz, 1H, *meta* Py′), 3.74 (d, J = 11 Hz, 1H, ArCH_2), 3.58 (d, J = 16 Hz, PyCH_2), 3.18 (d, J = 15 Hz, 1H, PyCH_2), 3.12 (d, J = 15 Hz, 1H, PyCH_2), 3.09 (d, J = 16 Hz, 1H, $PyCH_2$), 2.26 (d, J = 11 Hz, 1H, ArCH_2), 1.75 (s, 9H, *t*Bu), 1.40 (s, 9H, *t*Bu), 1.06 (bs, 9H, $SiMe_3$), 0.09 (bs, 9H, $SiMe_3$); $^{13}C\{^1H\}$ NMR (C_6D_6, 101 MHz): 164.8 (Ar), 154.0 (Py), 149.3 (Py), 137.7 (Py), 137.6 (Ar), 134.0 (Ar), 125.2 (Ar), 123.9 (Ar), 123.1 (Py), 121.8 (Ar), 121.6 (Py), 62.3 (CH_2Ar), 61.1 (CH_2Py), 35.6 (CMe_3), 33.9 (CMe_3), 32.4 (CMe_3), 30.5 (CMe_3), 6.6 ($SiMe_3$). UV-vis (toluene, 5.7×10^{-5} M) [λ_{max}, nm (ε, mol^{-1} cm^2)]: 296 (4200). Anal. calcd for $C_{33}H_{52}N_4OSi_2Zn$: C, 61.70; H, 8.16; N, 8.72; anal. calcd for $C_{33}H_{52}ZnN_4OSi_2{\cdot}C_6H_{14}$: C, 64.30; H, 9.13; N, 7.69; found: C, 61.99; H, 8.79; N, 8.40 (X-ray structure shows presence of 1 co-crystallised hexane, which seems to be lost partly on drying. NMR shows the presence of 0.7 hexane, EA analysis samples best agree with 0.2 hexane).

***rac*-Lactide polymerisation.** In a glove box, the desired amount of *rac*-lactide was placed into a J.-Young tube together with C_6D_6. If required, a stock solution of an additive (EtOH, *etc.*) was added, followed by a stock solution of the catalyst (≈ 20 mM in C_6D_6). The reaction was followed by ^{1}H NMR. The reaction was quenched by addition of ≈5 equiv. of a $CDCl_3$ solution of acetic acid (5 mM). The volatiles were immediately evaporated and solid polymer samples were stored at −80 °C for further analysis. Conversion was determined from ^{1}H NMR by comparison to remaining lactide. P_m values were determined from homodecoupled ^{1}H NMR spectra and calculated from $P_m = 1 - 2{\cdot}I_1/(I_1 + I_2)$, with I_1 = 5.15–5.21 ppm (*rmr*, *mmr*/*rmm*), I_2 = 5.21–5.25 ppm (*mmr*/*rmm*, *mmm*, *mrm*). The integration of the left multiplet and right multiplet (I_1 and I_2) required only one, very reproducible dividing point of the integration, which was always taken as the minimum between the two multiplets. P_m-Values obtained this way were typically consistent to ±1% over the course of one experiment and ±3% between different experiments under identical conditions. Molecular weight analyses were performed on *crude reaction products* using a Waters 1525 gel permeation chromatograph equipped with three Phenomenex columns and a refractive index detector at 35 °C. THF was used as the eluent at a flow rate of 1.0 mL min^{-1} and poly-

Table 4 Experimental details of X-ray diffraction studies

	2	**(L1)$_2$Zn**	**8**	**9**	**11**
Formula	$C_{56}H_{56}Zn_2N_8O_2$	$C_{44}H_{44}ZnN_6$	$C_{25}H_{47}ZnN_3O$	$C_{29}H_{60}ZnN_4Si_2O$	$C_{39}H_{66}ZnN_4Si_2O$
M_w (g mol^{-1}); $d_{calcd.}$ (g cm^{-3})	1003.82; 1.312	722.22; 1.236	471.02; 1.125	602.36; 1.115	728.50; 1.155
T (K); F(000)	100; 2096	100; 760	150; 1024	150; 1312	150; 1576
Crystal system	Orthorhombic	Orthorhombic	Monoclinic	Triclinic	Monoclinic
Space group	$P2_12_12_1$	$P2_12_12$	$P2_1/c$	$P(\bar{1})$	$P2_1/c$
Unit cell: a (Å)	10.1814(3)	11.4428(7)	9.9872(6)	13.6954(8)	18.8720(5)
b (Å)	13.3856(4)	11.9319(8)	24.3367(16)	13.8027(8)	18.6906(5)
c (Å)	37.3018(12)	14.2169(9)	11.7387(7)	19.6030(11)	12.3226(3)
α (°)	90	90	90	78.331(3)	90
β (°)	90	90	102.843(2)	89.408(3)	105.3650(10)
γ (°)	90	90	90	81.562(3)	90
V (Å^3); Z	5083.6(3); 4	1941.1(2); 2	2781.8(3); 4	3589.0(4); 4	4191.18(19); 4
μ (mm^{-1}); Abs. Corr.	0.956; multiscan	0.725; multiscan	1.350; multiscan	1.115; multiscan	1.010; multiscan
θ range (°); completeness	3.1–60.7; 0.97	2.7–60.7; 1.0	5.3–71.4; 0.98	2.8–60; 1.0	3.0–60.6; 1.0
Collected reflections; R_σ	114 196; 0.0226	21 172; 0.0361	31 767; 0.0356	90 622; 0.0669	70 912; 0.0163
Unique reflections; R_{int}	11 290; 0.0487	4452; 0.0607	5351; 0.0454	16 482; 0.0904	9608; 0.0311
$R_1(F)$ ($I > 2\sigma(I)$)	0.0301	0.0361	0.0586	0.0644	0.0509
w$R(F^2)$ (all data)	0.0765	0.0909	0.2791	0.1660	0.1462
GoF(F^2); flack-x	1.054; 0.050(16)	1.120; 0.12(3)	1.271; —	1.021; —	1.044; —
Residual electron density	0.338; −0.391	0.336; −0.302	0.709; −1.162	0.640; −0.380	0.905; −0.751

styrene standards (Sigma–Aldrich, 1.5 mg mL^{-1}, prepared and filtered (0.2 mm) directly prior to injection) were used for calibration. Obtained molecular weights were corrected by a Mark–Houwink factor of 0.58.[91]

X-ray diffraction. Single crystals were obtained directly from isolation of the products as described above. Diffraction data were collected on a Bruker Venture METALJET diffractometer (Ga Kα radiation) or a Bruker APEXII with a Cu microsource/Quazar MX using the APEX2 software package.[92] Data reduction was performed with SAINT,[93] absorption corrections with SADABS.[94] Structures were solved by dual-space refinement (SHELXT).[95] All non-hydrogen atoms were refined anisotropic using full-matrix least-squares on F^2 and hydrogen atoms refined with fixed isotropic U using a riding model (SHELXL97).[96] Further experimental details can be found in Table 4 and in the ESI (CIF).†

Conflicts of interest

There are no conflicts to declare.

Acknowledgements

Funding was supplied by the NSERC discovery program (RGPIN-2016-04953) and the Centre for Green Chemistry and Catalysis (FQRNT). I. M. contributed during her research internship financed by the DAAD-RISE program. We thank Karine Gilbert, Marie-Christine Tang and Alexandra Furtos for support with mass spectroscopy and Francine Bélanger for support with X-ray crystallography.

Notes and references

1 V. Nagarajan, A. K. Mohanty and M. Misra, *ACS Sustainable Chem. Eng.*, 2016, **4**, 2899–2916.
2 E. Castro-Aguirre, F. Iñiguez-Franco, H. Samsudin, X. Fang and R. Auras, *Adv. Drug Delivery Rev.*, 2016, **107**, 333–366.
3 S. Slomkowski, S. Penczek and A. Duda, *Polym. Adv. Technol.*, 2014, **25**, 436–447.
4 T. A. Hottle, M. M. Bilec and A. E. Landis, *Polym. Degrad. Stab.*, 2013, **98**, 1898–1907.
5 S. Inkinen, M. Hakkarainen, A.-C. Albertsson and A. Södergård, *Biomacromolecules*, 2011, **12**, 523–532.
6 J. Ahmed and S. K. Varshney, *Int. J. Food Prop.*, 2011, **14**, 37–58.
7 C. K. Williams and M. A. Hillmyer, *Polym. Rev.*, 2008, **48**, 1–10.
8 B. Gupta, N. Revagade and J. Hilborn, *Prog. Polym. Sci.*, 2007, **32**, 455–482.
9 E. T. H. Vink, K. R. Rábago, D. A. Glassner, B. Springs, R. P. O'Connor, J. Kolstad and P. R. Gruber, *Macromol. Biosci.*, 2004, **4**, 551–564.
10 R. E. Drumright, P. R. Gruber and D. E. Henton, *Adv. Mater.*, 2000, **12**, 1841–1846.
11 M. Singhvi and D. Gokhale, *RSC Adv.*, 2013, **3**, 13558–13568.
12 J. Vijayakumar, R. Aravindan and T. Viruthagiri, *Chem. Biochem. Eng. Q.*, 2008, **22**, 245–264.
13 Y. Tokiwa and B. P. Calabia, *Can. J. Chem.*, 2008, **86**, 548–555.
14 B. J. O'Keefe, M. A. Hillmyer and W. B. Tolman, *J. Chem. Soc., Dalton Trans.*, 2001, 2215–2224, DOI: 10.1039/b104197p.
15 O. Dechy-Cabaret, B. Martin-Vaca and D. Bourissou, *Chem. Rev.*, 2004, **104**, 6147–6176.
16 Z. Zhong, P. J. Dijkstra and J. Feijen, *J. Biomater. Sci., Polym. Ed.*, 2004, **15**, 929–946.
17 J. Wu, T.-L. Yu, C.-T. Chen and C.-C. Lin, *Coord. Chem. Rev.*, 2006, **250**, 602–626.
18 A. Amgoune, C. M. Thomas and J.-F. Carpentier, *Pure Appl. Chem.*, 2007, **79**, 2013–2030.
19 R. H. Platel, L. M. Hodgson and C. K. Williams, *Polym. Rev.*, 2008, **48**, 11–63.
20 C. A. Wheaton, P. G. Hayes and B. J. Ireland, *Dalton Trans.*, 2009, 4832–4846.
21 N. Ajellal, J.-F. Carpentier, C. Guillaume, S. M. Guillaume, M. Helou, V. Poirier, Y. Sarazin and A. Trifonov, *Dalton Trans.*, 2010, **39**, 8363.
22 M. D. Jones, in *Heterogenized Homogeneous Catalysts for Fine Chemicals Production*, ed. P. Barbaro and F. Liguori, Springer Netherlands, 2010, vol. 33, pp. 385–412.
23 M. K. Kiesewetter, E. J. Shin, J. L. Hedrick and R. M. Waymouth, *Macromolecules*, 2010, **43**, 2093–2107.
24 M. J. Stanford and A. P. Dove, *Chem. Soc. Rev.*, 2010, **39**, 486–494.
25 A. K. Sutar, T. Maharana, S. Dutta, C.-T. Chen and C.-C. Lin, *Chem. Soc. Rev.*, 2010, **39**, 1724–1746.
26 C. M. Thomas, *Chem. Soc. Rev.*, 2010, **39**, 165.
27 J.-C. Buffet and J. Okuda, *Polym. Chem.*, 2011, **2**, 2758–2763.
28 S. Dagorne, C. Fliedel and P. de Frémont, in *Encyclopedia of Inorganic and Bioinorganic Chemistry*, John Wiley & Sons, Ltd, 2011, DOI: 10.1002/9781119951438.eibc2416.
29 P. J. Dijkstra, H. Du and J. Feijen, *Polym. Chem.*, 2011, **2**, 520–527.
30 S. Dutta, W.-C. Hung, B.-H. Huang and C.-C. Lin, in *Synthetic Biodegradable Polymers*, ed. B. Rieger, A. Künkel, G. W. Coates, R. Reichardt, E. Dinjus and T. A. Zevaco, Springer-Verlag, Berlin, 2011, pp. 219–284.
31 C. A. Wheaton and P. G. Hayes, *Comments Inorg. Chem.*, 2011, **32**, 127–162.
32 I. dos Santos Vieira and S. Herres-Pawlis, *Eur. J. Inorg. Chem.*, 2012, **2012**, 765–774.
33 J.-F. Carpentier, B. Liu and Y. Sarazin, in *Advances in Organometallic Chemistry and Catalysis*, John Wiley & Sons, Inc., 2013, pp. 359–378, DOI: 10.1002/9781118742952.ch28.
34 S. Dagorne and C. Fliedel, in *Modern Organoaluminum Reagents: Preparation, Structure, Reactivity and Use*,

ed. S. Woodward and S. Dagorne, Springer Berlin Heidelberg, Berlin, Heidelberg, 2013, pp. 125–171, DOI: 10.1007/3418_2012_35.
35 S. Dagorne, M. Normand, E. Kirillov and J.-F. Carpentier, *Coord. Chem. Rev.*, 2013, **257**, 1869–1886.
36 B. H. Huang, S. Dutta and C. C. Lin, in *Comprehensive Inorganic Chemistry II (Second Edition)*, ed. J. R. Poeppelmeier, Elsevier, Amsterdam, 2013, pp. 1217–1249, DOI: 10.1016/B978-0-08-097774-4.00146-7.
37 R. Jianming, X. Anguo, W. Hongwei and Y. Hailin, *Des. Monomers Polym.*, 2013, **17**, 345–355.
38 A. Sauer, A. Kapelski, C. Fliedel, S. Dagorne, M. Kol and J. Okuda, *Dalton Trans.*, 2013, **42**, 9007–9023.
39 S. M. Guillaume, E. Kirillov, Y. Sarazin and J.-F. Carpentier, *Chem. – Eur. J.*, 2015, **21**, 7988–8003.
40 J. P. MacDonald and M. P. Shaver, in *Green Polymer Chemistry: Biobased Materials and Biocatalysis*, American Chemical Society, 2015, vol. 1192, ch. 10, pp. 147–167.
41 S. Paul, Y. Zhu, C. Romain, R. Brooks, P. K. Saini and C. K. Williams, *Chem. Commun.*, 2015, **51**, 6459–6479.
42 E. Le Roux, *Coord. Chem. Rev.*, 2016, **306**, 65–85.
43 T. M. Ovitt and G. W. Coates, *J. Am. Chem. Soc.*, 2002, **124**, 1316–1326.
44 H. Du, A. H. Velders, P. J. Dijkstra, J. Sun, Z. Zhong, X. Chen and J. Feijen, *Chem. – Eur. J.*, 2009, **15**, 9836–9845.
45 K. Press, I. Goldberg and M. Kol, *Angew. Chem., Int. Ed.*, 2015, **54**, 14858–14861.
46 H. Ma, T. P. Spaniol and J. Okuda, *Angew. Chem., Int. Ed.*, 2006, **45**, 7818–7821.
47 A. Amgoune, C. M. Thomas, T. Roisnel and J.-F. Carpentier, *Chem. – Eur. J.*, 2006, **12**, 169–179.
48 A. J. Chmura, C. J. Chuck, M. G. Davidson, M. D. Jones, M. D. Lunn, S. D. Bull and M. F. Mahon, *Angew. Chem., Int. Ed.*, 2007, **46**, 2280–2283.
49 A. J. Chmura, M. G. Davidson, C. J. Frankis, M. D. Jones and M. D. Lunn, *Chem. Commun.*, 2008, 1293–1295.
50 M. D. Jones, S. L. Hancock, P. McKeown, P. M. Schafer, A. Buchard, L. H. Thomas, M. F. Mahon and J. P. Lowe, *Chem. Commun.*, 2014, **50**, 15967–15970.
51 M. D. Jones, L. Brady, P. McKeown, A. Buchard, P. M. Schafer, L. H. Thomas, M. F. Mahon, T. J. Woodman and J. P. Lowe, *Chem. Sci.*, 2015, **6**, 5034–5039.
52 S. Fortun, P. Daneshmand and F. Schaper, *Angew. Chem., Int. Ed.*, 2015, **54**, 13669–13672.
53 P. Daneshmand, A. van der Est and F. Schaper, *ACS Catal.*, 2017, **7**, 6289–6301.
54 P. Daneshmand, S. Fortun and F. Schaper, *Organometallics*, 2017, **36**, 3860–3877.
55 P. Daneshmand, J. L. Jiménez-Santiago, M. Aragon–Alberti and F. Schaper, *Organometallics*, 2018, **37**, 1751–1759.
56 M. Cheng, A. B. Attygalle, E. B. Lobkovsky and G. W. Coates, *J. Am. Chem. Soc.*, 1999, **121**, 11583–11584.
57 T. M. Ovitt and G. W. Coates, *J. Am. Chem. Soc.*, 1999, **121**, 4072–4073.
58 F. Drouin, P. O. Oguadinma, T. J. J. Whitehorne, R. E. Prud'homme and F. Schaper, *Organometallics*, 2010, **29**, 2139–2147.
59 L. Wang and H. Ma, *Dalton Trans.*, 2010, **39**, 7897.
60 C.-Y. Sung, C.-Y. Li, J.-K. Su, T.-Y. Chen, C.-H. Lin and B.-T. Ko, *Dalton Trans.*, 2012, **41**, 953–961.
61 M. Honrado, A. Otero, J. Fernández-Baeza, L. F. Sánchez-Barba, A. n. Lara-Sánchez, J. Tejeda, M. a. P. Carrión, J. Martínez-Ferrer, A. Garcés and A. M. Rodríguez, *Organometallics*, 2013, **32**, 3437–3440.
62 H. Wang and H. Ma, *Chem. Commun.*, 2013, **49**, 8686–8688.
63 S. Abbina and G. Du, *ACS Macro Lett.*, 2014, **3**, 689–692.
64 M. Honrado, A. Otero, J. Fernández-Baeza, L. F. Sánchez-Barba, A. Garcés, A. n. Lara-Sánchez and A. M. Rodríguez, *Organometallics*, 2014, **33**, 1859–1866.
65 Z. Mou, B. Liu, M. Wang, H. Xie, P. Li, L. Li, S. Li and D. Cui, *Chem. Commun.*, 2014, **50**, 11411–11414.
66 H. Wang, Y. Yang and H. Ma, *Macromolecules*, 2014, **47**, 7750–7764.
67 M. Honrado, A. Otero, J. Fernández-Baeza, L. F. Sánchez-Barba, A. Garcés, A. Lara-Sánchez, J. Martínez-Ferrer, S. Sobrino and A. M. Rodríguez, *Organometallics*, 2015, **34**, 3196–3208.
68 Y. Sun, Y. Cui, J. Xiong, Z. Dai, N. Tang and J. Wu, *Dalton Trans.*, 2015, **44**, 16383–16391.
69 Y. Yang, H. Wang and H. Ma, *Inorg. Chem.*, 2015, **54**, 5839–5854.
70 T. Rosen, Y. Popowski, I. Goldberg and M. Kol, *Chem. – Eur. J.*, 2016, **22**, 11533–11536.
71 H. Wang, Y. Yang and H. Ma, *Inorg. Chem.*, 2016, **55**, 7356–7372.
72 C. Kan, J. Hu, Y. Huang, H. Wang and H. Ma, *Macromolecules*, 2017, **50**, 7911–7919.
73 D. E. Stasiw, A. M. Luke, T. Rosen, A. B. League, M. Mandal, B. D. Neisen, C. J. Cramer, M. Kol and W. B. Tolman, *Inorg. Chem.*, 2017, **56**, 14366–14372.
74 A. W. Addison, T. N. Rao, J. Reedijk, J. van Rijn and G. C. Verschoor, *J. Chem. Soc., Dalton Trans.*, 1984, 1349–1356, DOI: 10.1039/DT9840001349.
75 C. R. Groom, I. J. Bruno, M. P. Lightfoot and S. C. Ward, *Acta Crystallogr., Sect. B: Struct. Sci., Cryst. Eng. Mater.*, 2016, **72**, 171–179.
76 C. K. Williams, L. E. Breyfogle, S. K. Choi, W. Nam, V. G. Young, M. A. Hillmyer and W. B. Tolman, *J. Am. Chem. Soc.*, 2003, **125**, 11350–11359.
77 P. D. Knight, A. J. P. White and C. K. Williams, *Inorg. Chem.*, 2008, **47**, 11711–11719.
78 Z. Zheng, G. Zhao, R. Fablet, M. Bouyahyi, C. M. Thomas, T. Roisnel, O. Casagrande Jr. and J.-F. Carpentier, *New J. Chem.*, 2008, **32**, 2279–2291.
79 S. Yann, P. Valentin, R. Thierry and C. Jean-François, *Eur. J. Inorg. Chem.*, 2010, **2010**, 3423–3428.
80 V. Poirier, T. Roisnel, J.-F. Carpentier and Y. Sarazin, *Dalton Trans.*, 2011, **40**, 523–534.
81 T. Ebrahimi, E. Mamleeva, I. Yu, S. G. Hatzikiriakos and P. Mehrkhodavandi, *Inorg. Chem.*, 2016, **55**, 9445–9453.

82 D. Jedrzkiewicz, D. Kantorska, J. Wojtaszak, J. Ejfler and S. Szafert, *Dalton Trans.*, 2017, **46**, 4929–4942.
83 S. M. Kirk, P. McKeown, M. F. Mahon, G. Kociok-Köhn, T. J. Woodman and M. D. Jones, *Eur. J. Inorg. Chem.*, 2017, **2017**, 5417–5426.
84 G. Labourdette, D. J. Lee, B. O. Patrick, M. B. Ezhova and P. Mehrkhodavandi, *Organometallics*, 2009, **28**, 1309–1319.
85 S. C. Marinescu, T. Agapie, M. W. Day and J. E. Bercaw, *Organometallics*, 2007, **26**, 1178–1190.
86 M. Cheng, D. R. Moore, J. J. Reczek, B. M. Chamberlain, E. B. Lobkovsky and G. W. Coates, *J. Am. Chem. Soc.*, 2001, **123**, 8738–8749.
87 R. J. Herolds, L. Aggarwal and V. Neff, *Can. J. Chem.*, 1963, **41**, 1368.
88 D. Y. Lee and J. F. Hartwig, *Org. Lett.*, 2005, **7**, 1169–1172.
89 S. Mondal, S. M. Mandal, T. K. Mondal and C. Sinha, *Spectrochim. Acta, Part A*, 2015, **150**, 268–279.
90 M. Savva, P. Chen, A. Aljaberi, B. Selvi and M. Spelios, *Bioconjugate Chem.*, 2005, **16**, 1411–1422.
91 M. Save, M. Schappacher and A. Soum, *Macromol. Chem. Phys.*, 2002, **203**, 889–899.
92 *APEX2, Release 2.1-0*, Bruker AXS Inc., Madison, USA, 2006.
93 *SAINT, Release 7.34A*, Bruker AXS Inc., Madison, USA, 2006.
94 G. M. Sheldrick, *SADABS*, Bruker AXS Inc., Madison, USA, 1996 & 2004.
95 G. Sheldrick, *Acta Crystallogr. Sect. A: Found. Adv.*, 2015, **71**, 3–8.
96 G. M. Sheldrick, *Acta Crystallogr., Sect. A: Found. Crystallogr.*, 2008, **64**, 112–122.